Available online at www.sciencedirect.com
ScienceDirect
Journal of Magnetic Resonance 182 (2006) 75–83
JMR Journal of Magnetic Resonance
www.elsevier.com/locate/jmr

A practical and flexible implementation of 3D MRI in the Earth's magnetic field

Meghan E. Halse [a,b], Andrew Coy [b], Robin Dykstra [c], Craig Eccles [b], Mark Hunter [a], Rob Ward [c], Paul T. Callaghan [a,*]

[a] MacDiarmid Institute for Advanced Materials and Nanotechnology, Victoria University of Wellington, Wellington, New Zealand
[b] Magritek Limited, Wellington, New Zealand
[c] Institute of Fundamental Sciences, Massey University, Palmerston North, New Zealand

Received 30 March 2006; revised 5 June 2006
Available online 7 July 2006

Abstract

The Earth's magnetic field, though weak, is appealing for NMR applications because it is highly homogeneous, globally available and free. However, the practicality of Earth's field NMR (EFNMR) has long been limited by the need to perform experiments in outdoor locations where the local field homogeneity is not disrupted by ferrous or magnetic objects and where ultra-low frequency (ULF) noise sources are at a minimum. Herein we present a flexible and practical implementation of MRI in the Earth's magnetic field that demonstrates that EFNMR is not as difficult as it was previously thought to be. In this implementation, pre-polarization and ULF noise shielding, achieved using a crude electromagnet, are used to significantly improve signal-to-noise ratio (SNR) even in relatively noisy environments. A three axis gradient coil set, in addition to providing imaging gradients, is used to provide first-order shims such that sub-hertz linewidths can routinely be achieved, even in locations of significant local field inhomogeneity such as indoor scientific laboratories. Temporal fluctuations in the magnitude of the Earth's magnetic field are measured and a regime found within which these variations in Larmor frequency produce no observable artefacts in reconstructed images.

Keywords: MRI; Imaging; EFNMR; Earth's magnetic field

1. Introduction

In recent years there has been a mounting interest in nuclear magnetic resonance (NMR) performed at low detection field strengths. The growth of interest in this field can be attributed to the wide range of potential applications for portable and/or *ex situ* NMR and MRI systems [1,2].

In the sense of convenience of use and uniformity of field, Earth's field NMR (EFNMR) can be considered to be the ultimate low-field experiment. However, lower field NMR experiments are possible using field cancellation coils to counter the Earth's field and superconducting quantum interference devices (SQUIDs) for detection [3]. EFNMR holds significant interest as an academic concept but, for practical reasons, has traditionally been limited to remote outdoor environments [4–11], i.e. locations far from any disruptions to the local homogeneity of the Earth's magnetic field and sources of ULF noise. Recently there have been some remarkable demonstrations of the potential utility of EFNMR [12–16]. For example, Mohoric et al. [13,14] have demonstrated 2D imaging in the Earth's magnetic field and also self-diffusion weighted imaging and velocity imaging. Even more recently, Appelt et al. [15] have demonstrated astonishingly high-resolution *J*-coupling spectra for a number of organic molecules acquired in the Earth's magnetic field.

These experiments suggest that the full potential of EFNMR has yet to be tapped, although the practicality

* Corresponding author. Fax: +64 6 350 5164.
E-mail address: Paul.Callaghan@vuw.ac.nz (P.T. Callaghan).

1090-7807/$ - see front matter © 2006 Elsevier Inc. All rights reserved.
doi:10.1016/j.jmr.2006.06.011

of this methodology is limited by the need to perform experiments outdoors. In this communication we present a flexible, direct-detection approach to MRI in the Earth's magnetic field that can be carried out inside the laboratory and a wide range of non-idealized environments.

2. Theory

The various methodologies employed to achieve MRI in the Earth's magnetic field are well known from traditional high-field MRI applications. The interesting features of Earth's field MRI and the unique challenges presented by its implementation arise not from the pulse sequences employed but rather from the very nature of the Earth's magnetic field (B_E) itself. The magnitude of the Earth's field is on the order of 50 μT, giving rise to Larmor frequencies of approximately 2 kHz for protons. This Larmor frequency, lying in the ultra-low frequency (ULF) band (300 Hz–3 kHz), presents both a challenge and an opportunity. The challenge arises from the extremely low thermal polarization available at 50 μT and the wide range of non-negligible ULF noise sources in typical laboratory environments; the opportunity arises from access to a highly uniform detection field and the ability to use direct detection and simple low-frequency electronics.

Another feature of the Earth's magnetic field that presents a challenge to NMR and MRI alike is that there exist temporal changes in the magnitude of B_E on the order of tens of nanotesla, changes which can occur on a time scale of hours or even minutes. These daily, or diurnal, variations are caused by electric currents induced in the Earth by currents in the ionosphere [17]. This temporal instability of the detection field can introduce a frequency shift and phase drift between successive lines in k-space resulting in artefacts in the reconstructed image.

2.1. Fluctuations in the magnitude of the Earth's field

In the previous work by Mohoric et al. [13,14], a reference coil, coupled with heterodyne detection, was used to compensate for any drift in the Larmor frequency during an imaging experiment. We will show here that a much simpler approach, in which field drifts are measured and experimental time limits set, proves highly effective and that no such signal reference method is needed.

Fluctuations in the Earth's magnetic field can be measured by EFNMR using a large bulk water sample and a simple polarize, pulse and collect experiment. Following a pre-polarizing pulse, the magnetization is excited by a B_1 pulse and allowed to evolve in the Earth's magnetic field for a time t prior to FID acquisition. The spectral peak in the corresponding spectrum can then be "phased" to obtain a signal phase value, ϕ. Fluctuations in the magnitude of the Earth's field can be tracked by repeating this experiment at regular time intervals. Changes in the magnitude of the Earth's field, ΔB_E, at each time step, j, can be calculated relative to the first measurement as:

$$\Delta B_E(\phi_j) = \frac{\phi_j - \phi_1}{\gamma t}, \tag{1}$$

where t is the phase evolution time between excitation and detection of the signal and γ is the gyromagnetic ratio. The parameter t must be chosen carefully to avoid phase wrap problems. An appropriate value of t can be chosen based on an estimate of the maximum change in B_E, $\Delta B_{E(max)}$, using to the following relation:

$$t = \frac{2\pi}{\gamma \Delta B_{E(max)}}.$$

In order to determine the effect of this temporal change in B_E on an image, consider the effect of small changes in Larmor frequency, $\Delta\omega_n$, on a typical two dimensional imaging experiment, where n is an integer denoting the phase encode gradient step.

First we consider fluctuations in B_E on a time scale of milliseconds. Such fluctuations, occurring during the acquisition of a single transient, will cause a broadening of the line in the frequency domain and therefore limit the minimum achievable frequency resolution in the read dimension of an image. The extent of this broadening, and hence the frequency limitation, can be assessed using the acquisition of a single transient and observing the resultant frequency spectrum.

Next we consider the longer time fluctuations, occurring over minutes and hours. For the purpose of a discussion of these longer characteristic time fluctuations we define a phase evolution time, t_0. This is the time during which the spins acquire a phase offset due to the frequency shift, $\Delta\omega_n$. This phase evolution time is dependent on the imaging pulse sequence employed.

Let t be the time as measured from the centre of the echo signal, τ_E be the time between the 90° and 180° pulses, G_x be the read gradient amplitude and k_y be the k-space encoding vector in the primary phase encode direction. The signal, as a function of $t$and k_y, can thus be written as:

$$S_n(t, k_y) = \int\int \rho(x, y) e^{i\gamma G_x x t} e^{i\Delta\omega_n (t+t_0)} e^{i2\pi k_y y}\, dx\, dy. \tag{2}$$

In the read direction the k-space encoding vector is defined as:

$$k_x = \frac{1}{2\pi}\gamma G_x t.$$

Therefore the signal can be re-written as:

$$S_n(k_x, k_y) = \int\int \rho(x, y) e^{i2\pi k_x (x + \frac{\Delta\omega_n}{\gamma G_x})} e^{i\Delta\omega_n t_0} e^{i2\pi k_y y}\, dx\, dy. \tag{3}$$

Taking the inverse Fourier transform with respect to k_x yields the following expression:

$$F_{k_x}\{S_n(k_x, k_y)\} = \int \rho(x - \frac{\Delta\omega_n}{\gamma G_x}, y) e^{i\Delta\omega_n t_0} e^{i2\pi k_y y}\, dy. \tag{4}$$

Therefore the consequence of a shift in the Larmor frequency of $\Delta\omega_n$ between successive lines in k-space is a shift

of $\frac{\Delta\omega_n}{\gamma G_x}$ in the image space read dimension and a phase shift of $\Delta\omega_n t_0$.

Consider first the effect on the read dimension. The pixel size, Δx, is given by the field of view (FOV_x) divided by the number of points in the read dimension (N_{read}). If the shift in the image due to drift in the Earth's magnetic field is less than the pixel size then no image artefacts will result from this shift. Therefore we require:

$$\frac{\Delta\omega_n}{\gamma G_x} < \frac{\mathrm{FOV}_x}{N_{\mathrm{read}}}. \tag{5}$$

If we consider the magnitude of the Earth's field to have a maximum rate of change with respect to time then we can define a maximum rate of change with respect to time of the Larmor frequency $\frac{\mathrm{d}f}{\mathrm{d}t} = \frac{\gamma}{2\pi}\left|\frac{\mathrm{d}B_{\mathrm{E}}}{\mathrm{d}t}\right|$. This quantity can be used to define the following condition for the maximum total experiment time, $T_{\max}$:

$$T_{\max} < \frac{\gamma G_x \mathrm{FOV}_x}{2\pi \dot{f} N_{\mathrm{read}}} = \frac{1}{t_{acq}\frac{\mathrm{d}f}{\mathrm{d}t}}, \tag{6}$$

where the simplified form on the right-hand side uses the following expression for the read gradient strength:

$$G_x = \frac{2\pi N_{\mathrm{read}}}{\gamma t_{acq} \mathrm{FOV}_x}. \tag{7}$$

Now consider the phase encode dimensions. The phase shift $\Delta\omega_n t_0$ is proportional to the time t_0 and therefore is dependent on the choice of pulse sequence. Consider the two pulse sequences in Fig. 1. In the case of the spin-echo pulse sequence (Fig. 1a) the phase offset acquired during the first τ_{E} time period is unwound for all frequencies during the second τ_{E} time period, following the 180° pulse. Therefore the phase evolution time, t_0, is zero. Consequently, for spin-echo imaging we need only be concerned with the read dimension shift (Eq. (6)). In the case of the gradient-echo pulse sequence (Fig. 1b) a phase offset due to a change in the Larmor frequency is acquired throughout the τ_{E} time period between excitation and the centre of the echo. Thus $t_0 = \tau_{\mathrm{E}}$ and the phase offset term is non-zero. We require that the phase drift over the whole experiment is much less than 2π. Therefore we define a factor α, which takes values less than one, to quantify the extent to which the total phase drift must be less than 2π. The required value of α will be set by the available signal-to-noise ratio and the need to keep image artefacts below the noise level.

Accordingly, the total phase drift over the experiment must satisfy:

$$\Delta\omega_n \tau_{\mathrm{E}} < 2\pi\alpha, \tag{8}$$

In terms of the maximum rate of change of the Larmor frequency with respect to time, $\frac{\mathrm{d}f}{\mathrm{d}t} = \frac{\gamma}{2\pi}\left|\frac{\mathrm{d}B_{\mathrm{E}}}{\mathrm{d}t}\right|$, the maximum total experiment time for a gradient echo imaging sequence, $T_{\max}$, is given by:

$$T_{\max} < \frac{\alpha}{\tau_{\mathrm{E}}\frac{\mathrm{d}f}{\mathrm{d}t}}. \tag{9}$$

Notice that Eq. (9) has the same form as the read dimension constraint, Eq. (6), scaled by a factor β, where $\beta = \frac{t_{acq}}{\tau_{\mathrm{E}}}\alpha$. In the simplest implementation of gradient echo $t_{acq} = \tau_{\mathrm{E}}$ and so $\beta = \alpha$. However, it is common to reduce τ_{E} by employing a large amplitude, short duration initial gradient pulse followed by longer duration, low amplitude gradient pulse during echo acquisition. This is done to improve SNR and can also slightly improve the total experiment time constraint because in this case, $\tau_{\mathrm{E}} < t_{acq}$ and so β will be greater than α.

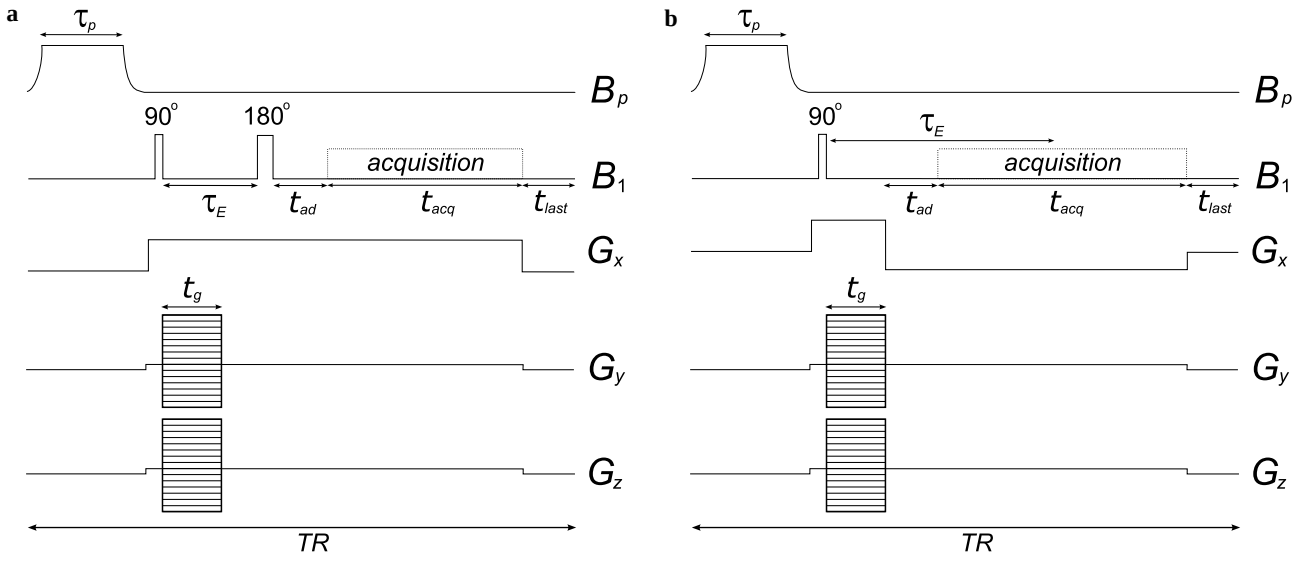

Fig. 1. Pulse sequence diagrams for imaging in the Earth's magnetic field using (a) spin-echoes and (b) gradient-echoes. The pulse sequences incorporate a pre-polarizing pulse of duration τ_{p} prior to each line in k-space. An acquisition delay, t_{ad}, typically 20 ms, is inserted between excitation and detection to allow for the ring down of the transmit/receive coil. Shim currents are output to the gradient coil between the polarizing pulse and the B_1 pulse and maintained throughout the excitation and detection time periods. All gradient pulses are superimposed on top of the shims.

The choice of the α factor is experiment specific. If there is a random distribution of phase shifts between lines in k-space, the image will suffer from ghosting artefacts in the phase dimension. If the phase shifts correspond to a linear change in Larmor frequency, the image will be stretched in the phase dimension. In the former case, if the smearing of image intensity is less than the baseline noise in the image then no artefacts will be observed. The SNR of the image will simply appear reduced. In the second case, if the extent of stretching in the phase dimension is small compared to the field of view then no artefacts will be observed.

2.2. Sensitivity

Setting limits on the total acquisition time to satisfy the requirements of field stability requires that the EFNMR instrument delivers sufficient signal-to-noise ratio; however, thermal polarization by B_E alone does not yield adequate signal. This sensitivity limitation can be overcome through the use of pre-polarization, a method first proposed by Packard and Varian in 1954 [18]. In this method, prior to the excitation and detection of the nuclear magnetization, a pre-polarizing field is applied to the system. This pre-polarizing field establishes an enhanced thermal polarization in the sample. The rate at which the spins are thermally polarized is a function of the T_1 of the spins in the polarizing field, B_p. After a time period of several T_1's we switch off the polarizing pulse adiabatically, i.e., slowly on the timescale of the precessing magnetization, such that the spins re-orient in the direction of the Earth's magnetic field while maintaining an increased level of polarization [6]. This enhanced magnetization can subsequently be manipulated with RF and gradient pulses in a manner similar to that used in the more traditional high field NMR and MRI pulse sequences. Fig. 1 shows two typical Earth's field MRI pulse sequence for spin-warp imaging which include polarizing pulses of duration τ_p.

In addition to enhancing thermal polarization, the pre-polarizing coil increases SNR by acting as a shield from external ULF noise sources [7]. This is achieved by shorting the polarizing coil during the excitation and detection stages of the pulse sequence. The polarizing coil is a solenoid with multiple layers of copper windings. On average the thickness of the copper is 10 mm. Thus it is a very good shield for ULF noise. If the external noise is directional, the shielding will be at its most effective at a very specific orientation. Any deviation from this orientation results in a dramatic increase in the observed noise on the NMR signal. Therefore the orientation of the long axis of the probe must be chosen according to noise shielding considerations. This orientation constraint has a consequence on the magnitude and orthogonality of the three axis imaging magnetic field gradients.

2.3. Orthogonality of imaging gradients

Another feature of the Earth's magnetic field that renders EFNMR different from traditional high-field magnetic resonance is the orientation of B_E, which for most locations on the planet is neither vertical nor horizontal but rather at a declination angle, d, to the vertical. This magnetic field orientation affects the magnitude and direction of the magnetic field gradients generated by the gradient coil set. In order to understand this problem we define two frames of reference: the laboratory frame, xyz, and the gradient coil set frame, $x'y'z'$. For simplicity, we define the x-axis of the laboratory frame such that it is aligned with x', which represents the long axis of the gradient coil set; however it is important to note that the relative alignment of the coil frame and the laboratory frame is arbitrary. The orientation of x'-axis of the gradient coil set is determined by noise considerations; therefore it is constrained to reorientation by rotation about the x-axis only.

The gradient coil set consists of a saddle coil and two quadrupolar coils 45° apart as in standard electromagnet geometry [19]. This arrangement generates three linear magnetic field gradients that operate in the weak gradient field approximation: $|\mathbf{B}_g| \ll B_E$. Ideally these gradients are orthogonal and are directed along x', y' and z', respectively; however, if the Earth's magnetic field vector does not point along z' in the gradient coil reference frame, non-orthogonal gradients will result.

Consider the situation presented in Fig. 2a where y' and z' are aligned with y and z. The magnetic field vector, $\mathbf{B_E}$, points at a declination angle, d, to the vertical and is at an angle ϕ to the y-axis in the horizontal plane. The magnetic field gradients $\mathbf{G_x}$, $\mathbf{G_y}$ and $\mathbf{G_z}$ generated by the gradient coil set in this orientation are non-orthogonal. Now consider the situation presented in Fig. 2b. The coil has been rotated about the x-axis such that $\mathbf{B_E}$ lies in the xz' plane, at an angle θ to the z'-axis. In this orientation, $\mathbf{G_y}$ and $\mathbf{G_z}$ will be directed along y' and z', respectively; however, $\mathbf{G_x}$ will be generated in the xz' plane, rotated away from the x-axis about the y'-axis by an angle θ . Therefore $\mathbf{G_y}$ is orthogonal with respect to both $\mathbf{G_z}$ and $\mathbf{G_x}$ but $\mathbf{G_x}$ and $\mathbf{G_z}$ will be non-orthogonal with respect to each other. The result is that a 3D MRI acquired with this gradient orientation will be geometrically correct in the xy and zy planes but will be skewed by an angle θ in the xz plane. If θ is well known, linear combinations of $\mathbf{G_x}$ and $\mathbf{G_z}$ can be used to generate two orthogonal gradients in the xz' plane. In addition to this non-orthogonality of the gradients, the magnitude of $\mathbf{G_y}$ and $\mathbf{G_z}$ will be reduced by a factor of $\cos\theta$.

2.4. Resolution

The final important issue involved in Earth's field MRI is the local homogeneity of the Earth's magnetic field. In order to maintain the weak gradient field approximation as well as to optimize image SNR, it is necessary to employ frequency encode gradients on the order of a few μT/m. Such weak gradients result in a very narrow frequency spread across the image. For example, with a typical field of view (FOV) of 100 mm and a read gradient of 7 μT/m, the frequency spread in the read dimension will be 30 Hz.

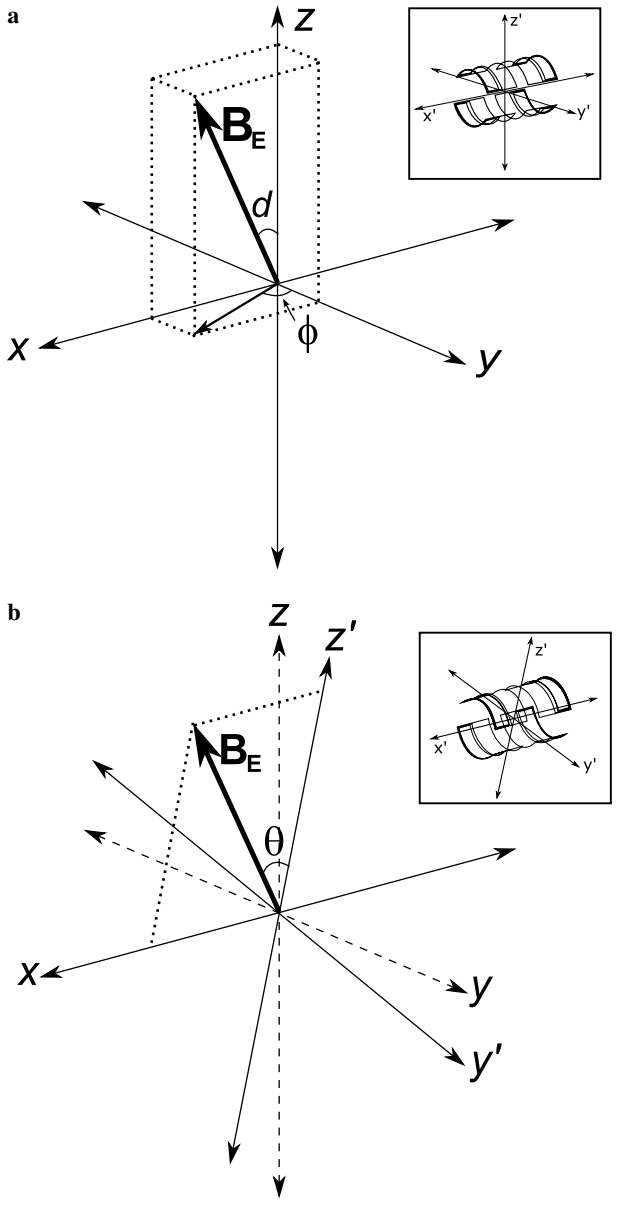

Fig. 2. The xyz-axes represent the three orthogonal dimensions of the laboratory frame, where z is vertical and x is the long axis of the gradient coil. The $x'y'z'$-axes represent the three orthogonal dimensions of the gradient coil frame. (a) Relative to the xyz frame, the Earth's magnetic field vector, $\mathbf{B_E}$, is oriented at a declination angle d, to the vertical, z, and the projection of $\mathbf{B_E}$ in the horizontal xy plane is at an angle, ϕ, to the y-axis. When the gradient coil is oriented such that x', y' and z' are aligned with x, y and z, respectively, the magnetic field gradients produced are non-orthogonal. (b) The gradient coil can be rotated about x such that $\mathbf{B_E}$ lies in the xz' plane. In this orientation, $\mathbf{G_y}$ is generated along y' with a magnitude reduced by $\cos\theta$ and similarly $\mathbf{G_z}$ is generated along the z' direction with a magnitude reduced by $\cos\theta$. $\mathbf{G_x}$ is generated in xz' plane at an angle of θ to the x-axis.

Consequently, in order to obtain reasonable image resolution sub-hertz linewidths are required.

In the absence of disruption by magnetic objects, the local homogeneity of the Earth's magnetic field is such that for a typical water sample, the linewidth will be T_2 limited and consequently on the order of half a hertz. However, in a less ideal situation the inhomogeneity of the local Earth's magnetic field can result in linewidths on the order of several Hz. It is possible to seek out naturally occurring locations of sufficient local homogeneity; however this approach greatly limits the range of places where the Earth's field technique can be implemented. Therefore we have implemented a method for using the three imaging gradients as first-order shims in order to compensate for any local field inhomogeneity. In this way, even in a location of significant disruption to the Earth's magnetic field homogeneity, sub-hertz linewidths can be obtained. A set of higher order shim coils can be designed to further improve the minimum achievable linewidths and also to broaden the range of locations where narrow linewidths can be obtained; however in this work the use of first-order shims proved to be highly effective and so higher order shims were not implemented.

3. Results/discussion

Fig. 3 presents the temporal fluctuations of B_E over a 42 h time period. These fluctuations were recorded both by EFNMR in Wellington, New Zealand and by a magnetometer in Eyrewell, New Zealand. The magnetometer data was obtained from the Institute of Geological and Nuclear Sciences Limited through the Intermagnet network website [20]. Although geographically separated by a few hundred kilometres, both of these measurements follow a similar pattern and magnitude of fluctuation.

The diurnal fluctuations are driven by solar wind [17] and therefore the magnitude of variation is much greater during the day than at night. The measurement in Fig. 3 was commenced in the early evening and so we observe a small magnitude fluctuation over the first 12 h of the

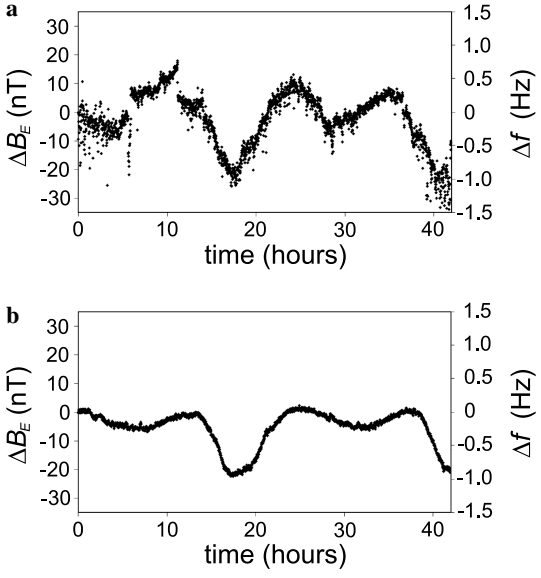

Fig. 3. Diurnal fluctuations in the magnitude of the Earth's magnetic field measured over a period of 42 h in (a) Wellington, New Zealand with EFNMR and (b) in Eyrewell, New Zealand using a magnetometer (20).

measurement followed by a larger magnitude fluctuation over the subsequent 12 h. The maximum daytime peak-to-peak amplitude of fluctuation is approximately 30 nT, which corresponds to a frequency shift of 1.3 Hz. This fluctuation occurs over a time period of 8 h. Therefore the maximum daytime rate of change of the frequency, $\frac{df}{dt}$, is on the order of 0.15 Hz per hour. The maximum night-time peak-to-peak fluctuation amplitude is approximately 15 nT, which corresponds to a frequency shift of 0.6 Hz. This shift occurs over a period of 6 h, resulting in a night-time rate of change of frequency on the order of 0.1 Hz per hour. Considering the total imaging time constraint in Eq. (6) this means that for a typical acquisition time of 2 s, the maximum total experiment time for a spin-echo measurement during the day is 3 h and 20 min and 5 h at night. Choosing an echo time, τ_E, of 1 s and $\alpha = 1/16$, the maximum total experiment time for a gradient echo measurement, as calculated from Eq. (9), is 25 min during the day and 37.5 min at night. These numbers indicate that it is possible to achieve imaging in the Earth's field without the need to compensate for the diurnal fluctuations in the magnitude of B_E.

The correlation between the EFNMR and magnetometer results presented in Fig. 3 implies that the major source of temporal instability in the magnitude of the Earth's magnetic field during the Wellington measurement was the solar driven diurnal fluctuation of the Earth's magnetic field. It is possible that for other locations there will be more dominant environment sources of temporal instability. In such cases, the fluctuations could potentially be more rapid or more severe than those originating from the geomagnetic diurnal fluctuations alone; however, the EFNMR experiment presented in this paper can be used to measure both the timescale and magnitude of any fluctuations in the magnitude of the Earth's magnetic field, irrespective of the source. The resultant values for the magnitude and timescale of the fluctuations can be used to determine the optimal acquisition time and maximum total image time such that Eq. (6) is fulfilled.

Prior to each imaging experiment, first-order shimming was achieved by passing very small currents, on the order of a few mA, through the three axis imaging magnetic field gradient coil. A simple polarize, pulse and collect experiment was employed to determine the ideal shim values for a particular location and orientation of the probe. In this experiment, a given set of shim values were output to the gradient coil between the end of the polarizing pulse and the application of the B_1 pulse and maintained throughout excitation and detection of an FID. The magnitude spectrum corresponding to this FID was used to determine the height of the sample peak, which was in turn used as a measure of the quality of the shim. An autoshim algorithm, employing a modified bisection approach, was used to iterate towards the ideal shim values by maximizing the height of this peak.

Results of a typical autoshim experiment are presented in Fig. 4. The line-width of the non-shimmed case (Fig. 4a) is 3.8 Hz. The linewidth of the shimmed case (Fig. 4b) is 0.3 Hz, showing a 12-fold increase in resolution. It is also evident from this experiment that shimming will greatly increase image SNR. The autoshim experiment took approximately 15 min.

All imaging pulse sequences incorporate the first-order shims by superimposing any gradient pulses on top of the base shim values. The shim values are switched on prior to signal excitation and maintained throughout the entire signal evolution and acquisition time periods. The pulse sequences shown in Fig. 1 demonstrate how shims are incorporated into typical imaging experiments.

A typical 3D MRI acquired in the Earth's magnetic field within a laboratory environment is shown in Fig. 5 as a rendered isosurface. The 3D image of a red capsicum was

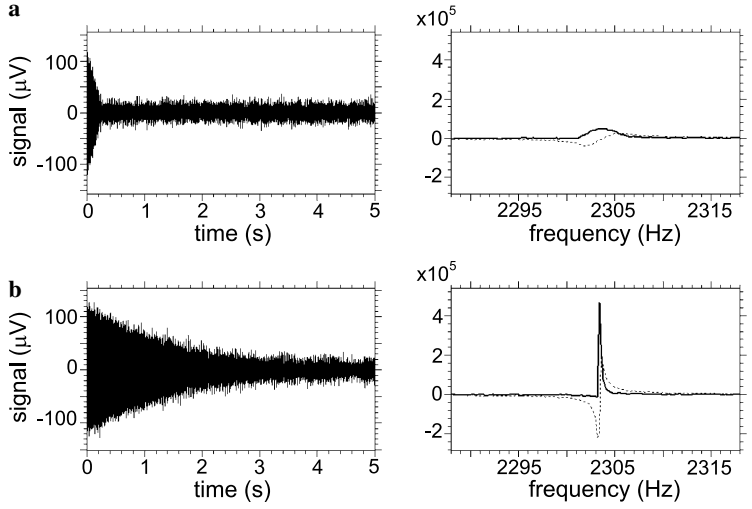

Fig. 4. (a) An FID acquired using EFNMR with no shimming. The linewidth is 3.8 Hz. (b) An FID acquired using EFNMR with shimming. The linewidth is 0.3 Hz showing a 12-fold increase in resolution. The shim values were obtained using an autoshim algorithm, which took approximately 15 min to complete.

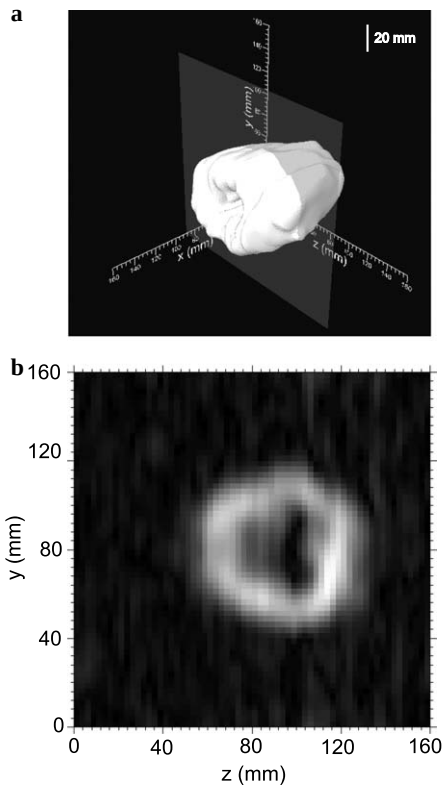

Fig. 5. (a) An isosurface rendering of a 3D MRI of a red capsicum acquired in the Earth's field using the spin-echo method illustrated in Fig. 1a. The polarizing time was 2 s with an average field strength of 18 mT. A broadband pulse of 1.5 ms duration was used to excite the entire sample. The repetition time was 5.5 s and the acquisition time was 2 s. The field of view was 160 mm isotropic with a matrix size of $32 \times 16 \times 16$ (zero-filled to 64 isotropic). Total imaging time was 1 h and 36 min. Four signal averages were employed. (b) A 2D slice of the 3D image taken along the plane shown in (a).

acquired using the spin-echo, spin-warp imaging sequence presented in Fig. 1a. The total image time was 1 h and 36 min. According to Eq. (6) the maximum total experiment time for a daytime spin-echo measurement with an acquisition time of 2 s is 3 h and 20 min. The total image time for the image presented in Fig. 5 falls considerably short of this critical limit and so we would not expect to observe image artefacts due to diurnal fluctuations in the Earth's field in this image. A 2D slice of the 3D image, taken along the plane indicated in Fig. 5a, is presented in Fig. 5b. A capsicum was chosen as an ideal sample for this experiment because of its favourable T_2 value ($\sim$1 s). Note that the observation window of Earth's field MRI requires samples to have $T_2 \geqslant 100$ ms, thus making human tissue imaging at Earth's field "a challenge".

In addition to the spin-echo imaging results shown, 2D/3D gradient-echo imaging and 2D filtered back projection imaging have also been achieved in the Earth's field within a laboratory environment.

In Earth's field MRI, repetition times (TRs) between the acquisition of successive lines in k-space are on the order of 10 s because in order to be effective, the pre-polarizing pulse requires a duration of several T_1 time periods and the T_1 of bulk water at Earth's field is approximately 2 s. Consequently the best way to improve the efficiency of imaging in the Earth's field is to acquire as many lines of k-space as possible following a single polarizing pulse. This naturally leads to the idea of using single-shot multiple echo techniques such as: echo-planar imaging (EPI) [21] or rapid-acquisition with relaxation enhancement (RARE) [22]. Single shot 2D imaging is challenging in the Earth's field because the T_2^* and T_2 decay of the signal is too rapid to allow for the acquisition of sufficient echoes to cover k-space in one sweep; however, multiple interleaved EPI or RARE acquisitions show promise for greatly increasing the speed of image acquisition at Earth's field.

4. Conclusions

In this work we have demonstrated that achieving MRI in the Earth's magnetic field is much easier than previously thought. Pre-polarization by an electromagnet and subsequent shorting of this pre-polarizing coil such that it acts as a ULF noise shield enhances the SNR to a sufficient extent that imaging can be achieved in reasonably short times, even in relatively noisy environments. These short imaging times make it possible to complete image acquisition in a total experiment time during which the temporal fluctuations in B_E do not manifest observable artefacts in the reconstructed image. In addition, the use of the three axis imaging gradients for first-order shimming facilitates improved resolution in areas of significant local field inhomogeneity, thus broadening the range of environments in which imaging can be achieved.

5. Experiment

The apparatus used to implement MRI in the Earth's magnetic field (Fig. 6a) is a modified Terranova Earth's field NMR system (magritek Limited, Wellington, NZ). The Terranova EFNMR probe consists of three concentric coils: a polarizing (B_p) coil, a gradient coil and a B_1 excitation/detection coil. The B_p and B_1 coils are coaxial solenoids and the gradient coil, used for diffusion measurements, is a collection of Maxwell and Helmholz turns. For the purposes of imaging, the probe was modified by the addition of a second gradient coil set. This set of coils consisted of a saddle coil to generate a gradient along the long axis of the coil, the x-axis, and two quadrupole coils at 45° to generate gradients in the y and z dimensions. An exploded view schematic of the probe is shown in Fig. 6b. Due to the very weak gradients required (on the order of μT/m) only small currents, on the order of tens of mA, are needed. Therefore it was possible to print the gradients onto 0.1 mm thick flexible PCB and wrap this sheet of PCB around the existing diffusion gradient coil within the Terranova apparatus. Thus the probe was modified for imaging without necessitating any modifications to its original structure.

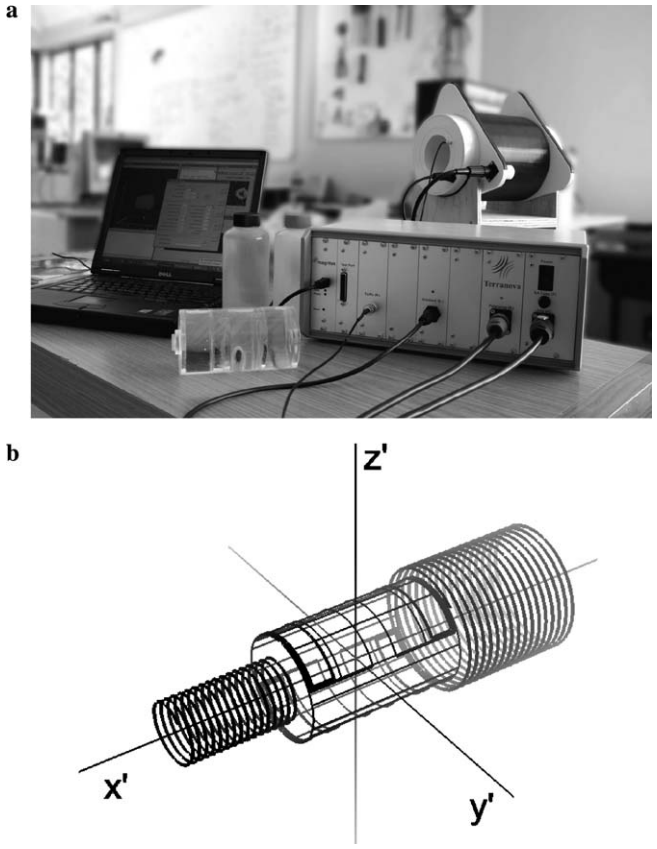

Fig. 6. (a) A photograph of the modified Terranova EFNMR apparatus that was used to perform MRI in the Earth's magnetic field. This system includes a controlling PC, a spectrometer and a three-coil probe. (b) An exploded view schematic of the three coil probe: an outer solenoid for pre-polarization, an inner solenoid for transmit and receive and a central imaging gradient coil set. The gradient coil set consists of two quadrupolar coils and a saddle coil. The original Terranova system was modified through the addition of the imaging gradient coil set and a three axis current source module. The imaging gradient coil set was printed on flexible PCB and wrapped around the existing diffusion gradient coil without necessitating any structural changes to the original probe. Within the spectrometer, the existing single axis current source, used for diffusion measurements, was replaced by the three axis current source used for imaging.

A Terranova EFNMR spectrometer was modified to allow for imaging by replacing the single current source used to drive the diffusion gradients with a three axis current source with a maximum available current of ± 300 mA, yielding a maximum gradient of approximately 80 μT/m. The modular nature of the spectrometer allowed for a simple replacement of the single current source with the three axis current source used for imaging.

All experiments were controlled by a PC connected to the spectrometer via a USB interface. The experiments were controlled and data was processed using the software package Prospa v2.0 (magritek Limited, Wellington, NZ).

Acknowledgments

This work was supported by funding from the New Zealand Foundation for Research, Science and Technology. M.E.H. acknowledges the support of a Victoria University of Wellington postgraduate scholarship. Dr. Gillian Turner and Dr. Malcolm Ingham are thanked for providing useful information on geomagnetism. Institute of Geological and Nuclear Sciences Ltd. is acknowledged for the magnetometer data made available on the Intermagnet website (www.intermagnet.org). Dafnis Vargas is thanked for help with photography and figure preparation.

References

[1] B. Blumich, F. Casanova, J. Perlo, S. Anferova, V. Anferov, K. Kremer, N. Goga, K. Kupferschlager, M. Adams, Advances of unilateral mobile NMR in non-destructive materials testing, Magn. Reson. Imaging 23 (2005) 197–201.
[2] Dimitris Sakellariou, Carlos A. Meriles, Alexander Pines, Advances in ex-situ nuclear magnetic resonance, C. R. Physique 5 (2004) 337–347.
[3] R. McDermott, A.H. Trabesinger, M. Műck, E.L. Hahn, A. Pines, J. Clarke, Liquid-State NMR and Scalar-Couplings in Microtesla Magnetic Fields, Science 295 (2002) 2247–2249.
[4] Bene GJ, 4 Int. S. Magn. Res. Reh. (1971).
[5] G.J. Bene, Nuclear magnetism of liquid-systems in the Earth's field range, Phys. Rep. 58 (1980) 213.
[6] P.T. Callaghan, M. Legros, Nuclear spins in the Earth's magnetic field, Am. J. Phys. 50 (1982) 709–713.
[7] P.T. Callaghan, C.D. Eccles, J.D. Seymour, An Earth's field nuclear magnetic resonance apparatus suitable for pulsed gradient spin echo measurements of self-diffusion under Antarctic conditions, Rev. Sci. Instrum. 68 (1997) 4263–4270.
[8] P.T. Callaghan, C.D. Eccles, T.G. Haskell, P.J. Langhorne, J.D. Seymour, Earth's field NMR in Antarctica: a pulsed gradient spin echo NMR study of restricted diffusion in sea ice, J. Magn. Reson. 133 (1998) 148–154.
[9] P.T. Callaghan, R. Dykstra, C.D. Eccles, T.G. Haskell, J.D. Seymour, A nuclear magnetic resonance study of Antarctic sea ice brine diffusivity, Cold Reg. Sci. Technol. 29 (1999) 153–171.
[10] O.R. Mercier, M.W. Hunter, P.T. Callaghan, Brine diffusion in first-year sea ice measured by Earth's field PGSE-NMR, Cold Reg. Sci. Technol. 42 (2005) 96–105.
[11] J.S. Brown Robert, Earth's field nuclear magnetic logging, Concept. Magnetic Res. 13 (2001) 344–366.
[12] J. Stepisnik, V. Erzen, M. Kox, NMR imaging in the Earth's magnetic-field, Magn. Reson. Med. 15 (1990) 386–391.
[13] Ales Mohoric, Gorazd Planinsic, Miha Kos, Andrej Duh, Janez Stepisnik, Magnetic resonance imaging system based on Earth's magnetic field, Instrum. Sci. Technol. 32 (2004) 655–667.
[14] Ales Mohoric, Janez Stepisnik, Miha Kos, Gorazd Planinsic, Self-diffusion imaging by spin echo in Earth's magnetic field, J. Magn. Reson. 136 (1999) 22–26.
[15] Stephan Appelt, Holger Kuhn, F. Wolfgang Hasing, Bernhard Blumich, Chemical analysis by ultrahigh-resolution nuclear magnetic resonance in the Earth's magnetic field, Nat. Phys. 2 (2006) 105–109.
[16] Stephan Appelt, F. Wolfgang Hasing, Holger Kuhn, Juan Perlo, Bernhard Blumich, Mobile high resolution xenon nuclear magnetic resonance spectroscopy in the Earth's magnetic field, Phys. Rev. Lett. 94 (2005) 197602.
[17] Ronald T. Merrill, Michael W. McElhinny, Phillip L. McFadden, The Magnetic Field of the Earth Paleomagnetism, the Core and the Deep Mantle, Academic Press, San Diego, 1998.
[18] M. Packard, R. Varian, Free nuclear induction in the Earth's magnetic field, Phys. Rev. 93 (1954) 941.

[19] Paul T. Callaghan, Principles of Nuclear Magnetic Resonance Spectroscopy, Oxford University Press, Oxford, 1991.
[20] Institute of Geological and Nuclear Sciences Ltd., Eyrewell, New Zealand, Intermagnet: International Real-Time Magnetic Observatory Network: <www.intermagnet.org/>.
[21] M.K. Stehling, R. Turner, P. Mansfield, Echo-planar imaging—Magnetic-resonance-imaging in a fraction of a second, Science 254 (1991) 43–50.
[22] J. Hennig, A. Nauerth, H. Friedberg, RARE imaging—A fast imaging method for clinical MR, Magn. Reson. Med. 3 (1986) 823–833.